Land Resources for Wind Energy Development Requires Regionalized Characterizations

Tao Dai[1,2], Jeya Maria Jose Valanarasu [3], Yifan Zhao[4], Shuwen Zheng[1], Yinong Sun[4], Vishal M Patel[2], Sarah M. Jordaan[5,6,*]

1. School of Advanced International Studies, Johns Hopkins University, Washington, DC, 20036, USA

2. Joint BioEnergy Institute, Lawrence Berkeley National Laboratory, Emeryville, CA 94608, USA

3. Department of Electrical and Computer Engineering, Johns Hopkins University, Baltimore, Maryland, 21218, USA

4. Department of Environmental Health and Engineering, Johns Hopkins University, Baltimore, Maryland, 21218, USA

5. Department of Civil Engineering, McGill University, Montreal, Quebec H3A 0G4, Canada

6. Trottier Institute of Sustainability in Engineering and Design, McGill University, Montreal, Quebec H3A 0G4, Canada

*__Corresponding author__: Sarah M Jordaan, Ph.D.

Email: sarah.jordaan@mcgill.ca

Competing Interest Statement: The authors declare no competing interest.

Keywords: Wind Power, Land Use, Machine Learning, Remote Sensing

Abstract

Estimates of the land area occupied by wind energy differ by orders of magnitude due to data scarcity and inconsistent methodology. We developed a method that combines machine learning-based imagery analysis and geographic information systems and examined the land area of 318 wind farms (15,871 turbines) in the U.S. portion of the Western Interconnection. We found that prior land use and human modification in the project area are critical for land-use efficiency and land transformation of wind projects. Projects developed in areas with little human modification have a land-use efficiency of 63.8±8.9 W/m^2 (mean±95% confidence interval) and a land transformation of 0.24±0.07 m^2/MWh while values for projects in areas with high human modification are 447±49.4 W/m^2 and 0.05±0.01 m^2/MWh, respectively. We show land resources for wind can be quantified consistently with our replicable method; a method that obviates >99% of the workload using machine learning. To quantify the peripheral impact of a turbine, buffered geometry can be used as a proxy for measuring land resources and metrics when a large enough impact radius is assumed (e.g., >4 times the rotor diameter). Our analysis provides a necessary first step towards regionalized impact assessment and improved comparisons of energy alternatives.

Keywords: Wind Energy; Machine Learning; Land Use; Environmental Impact Assessment; Image Segmentation; Geographical Information System; Remote Sensing; Life Cycle Assessment.

Synopsis: Macro-energy analyses lack data inventories necessary to accurately quantify land impacts of energy. Combining machine learning, geographic information systems, and energy systems analysis, this research quantifies and maps the direct land impacts of wind power across the U.S. Western Interconnection.

Graphic for Table of Contents (TOC)

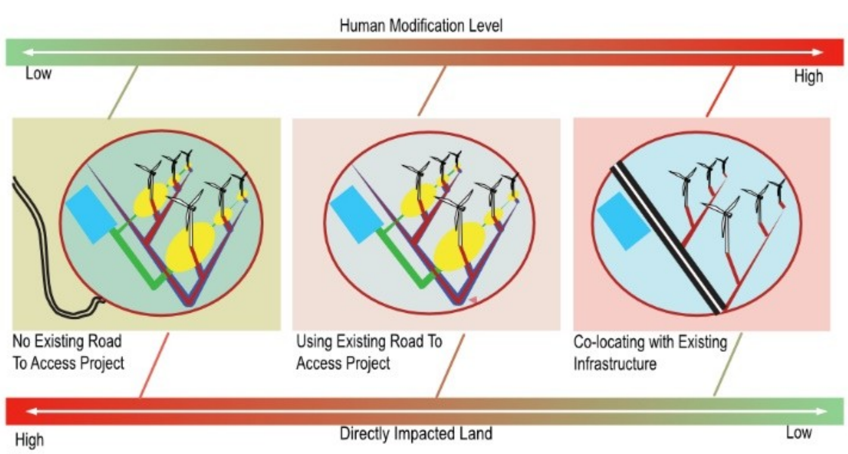

Introduction

Large-scale wind power is among the most important renewable and affordable alternatives to fossil fuels for achieving a decarbonized energy system.[1,2] Despite decarbonization benefits, the large extent of land required for the growth of wind power has been identified as a critical barrier to its deployment.[3–5] Compared to other energy technologies, wind power is perceived to have a relatively low capacity-based land-use efficiency (LUE), defined as the ratio of the nameplate capacity of a wind farm to its land requirement in W/m^2. Recent studies on wind farms have documented a capacity-based LUE of 4.3 W/m^2 (standard deviation = 3.5 W/m^2) (Harrison-Atlas et al. (2022)[6]) or as low as a mean of ~2 W/m^2 (Miller and Keith (2019)[7]), an order of magnitude lower than utility-scale solar PV.[8] Such estimates provide critical information for energy systems planning and decisions about future energy siting. However, it is widely acknowledged that land area directly impacted by wind energy development constitutes only a small fraction (typically <5%) of the total project area, as wind turbines are sited to optimize electricity generation from the kinetic energy of air in the free troposphere.[6,9,10] Wind farms often co-occur on landscapes with other human activities, such as agriculture. When accounting only the directly impacted land, LUE can be as high as 200 W/m^2.[11] The representativeness of LUE values is limited in energy systems planning due to the focus on the wind farm rather than the directly impacted land footprint.

Early studies that quantified relationship between wind energy and land in the U.S. were performed at relatively smaller scale.[12,13] Extrapolating such relationships at geospatial scales was therefore inappropriate and further challenged by the lack of publicly accessible project information (e.g., turbine location, turbine capacity, and turbine diameter).[14] One such early and foundational study examined land-wind energy interactions by assessing capacity-based LUE for both "total impacted" and "directly impacted" land using data from published environmental impact statements.[15] The authors defined the "total impacted" land as leased area used by the entire wind farm and the "directly impacted" land as the area disturbed by the wind turbines, access roads and other infrastructure.

More recently, the integration of imagery analysis and geographic information systems (GIS) has improved the quantification of relationships between energy developments and land. Geospatial methods have been used in the analyses of other energy infrastructure types[16–19] as they support a better understanding of land-use and land-cover change patterns across diverse geographies. Typical methods include manual delineation and geoprocessing. With manual delineation, an analyst delineates the boundaries of the different elements of an energy project, producing an annotated map of the directly impacted land. Diffendorfer and Compton (2014) applied manual delineation and conducted a detailed examination on how land cover, topography, and turbine configuration are related to the extent of land transformation.[20]

Geoprocessing, on the other hand, avoids the burden of mapping the directly impacted land and uses automatically generated zones (e.g., circular buffered zones, minimum bounding geometries and Thiessen polygons) around wind turbines as an approximation of impacted land. Large scale analysis to the extent of countries is possible with this approach[21–23] but results may not be accurate. Underestimation can occur when the analysis does not account for the full extent of the access roads. Overestimation can occur if the analysis neglects to account for land that was already developed prior to the construction of wind farms. For example, the geoprocessing approach may result in overestimated LUE estimates for the two following reasons. First, the buffered areas around turbines include land in use for agriculture that are not used by the turbines themselves. Second, the development of wind farms in these regions use existing roads networks, so the related infrastructure requires less new land (i.e., a land sparing opportunity).[24,25] While results using geoprocessing suggested that the LUE of wind has been decreasing over time,[6,7] Diffendorfer et al.[25] showed that new projects use existing road networks (with evidence from manual delineation) and thus require less new land. Systematic categorization of wind farms considering land cover type is thus needed to support a better understanding of impacts on lands with and without pre-existing infrastructure developments.

Manual delineation can be challenging and time consuming for energy infrastructure that requires a large population of facilities across extensive regions, such as wind turbines and natural gas production sites, especially when using high resolution imagery. For example, a previous study demonstrated that >130 hours is needed for the manual delineation of 60 km^2 of land use by natural gas production, which could represent the time of manual delineation needed for one wind farm, which has an median area of ~80 km^2 in the U.S.[6,26] As turbines with larger rotor diameter becoming more available, future workload of manual delineation could become greater as turbines needs to be spaced at a larger distance from each other. Advanced automatic delineating methods present enormous potential reducing the workload of quantifying directly impacted land of large-scale energy infrastructure, as shown in Dai et al. (2023), which quantifies the land use of natural gas production using a machine learning-based approach and reached a processing speed higher than 3.2 second/km^2.[27]

We introduce a novel automatic delineation approach based on computer vision and deep learning (hereafter, image segmentation) to map land directly impacted by wind farms at a large scale. Image segmentation is the task of assigning a pre-defined land-use class label (e.g., “Access Road”), to each pixel found in an image. Image segmentation has been widely applied to land-use quantification and land-cover classification, yet has primarily been used in energy studies focused on solar energy development.[28–32] We combined image segmentation with GIS analysis in a workflow that includes image preparation, image segmentation, and postprocessing for the accurate mapping of wind energy infrastructure. Results include the capacity-based LUE and land transformation (m^2/MWh). Land transformation is the ratio of land use to the life-time electricity generation of a power plant and facilitates a consistent comparison of land use for wind energy and other types of power generation technologies, from a life cycle perspective.[33] Our study provides a transparent and practical solution for determining the land area for large-scale wind energy infrastructure, extending the use of machine learning to new applications in energy systems analysis. Our approach and results will be a steppingstone to regionalized environmental impact assessments by providing a solid base for the evaluation of the land-use impacts in areas with varying levels of human development. Such information has implications for life cycle assessment (LCA)—a cradle-to-grave analysis of the environmental burdens of products and processes—which mainly relies on background literature or limited inventories to quantify land impacts.[34] LCA has been advancing in its capacity to incorporate spatiotemporal information into environmental impact methods for land,[35,36] which have been challenged by the lack of spatially explicit inventories.[37,38] More recently, a life cycle inventory for all power plants in the United States has been developed; yet, spatially explicit land-use data remains limited.[39,40] Impact assessments for wind energy development on ecosystems, landscape, and ecosystem services also require spatially explicit data and high resolution maps.[41,42,43,44] Results here are presented in terms of LUE (W/m2) but also provided in a format for broader applicability that includes energy systems planning and LCA.

Materials and Methods

Study Area and Data Sources. Our study area is the U.S. part of the Western Interconnection (Figure 1a).[45,46] Wind turbine locations and attributes were sourced from the US Wind Turbine Database,[14] and projects that were constructed between 1981 and 2018 were included in this study. Aerial imageries with a resolution of 1 meter or less acquired in 2018 from the National

Agriculture Imagery Program (NAIP) are used when applicable, and images from 2017 or 2019 when required since NAIP are typically collected every other year (image sources are documented in Supporting Data).

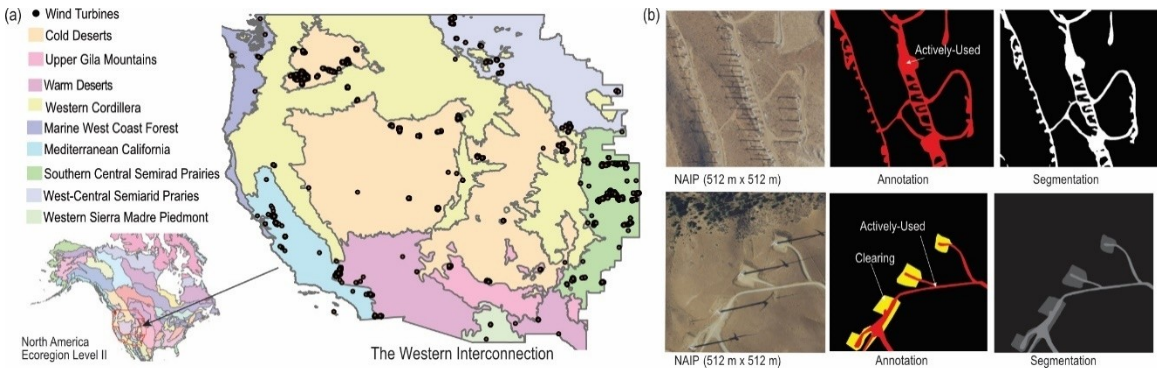

Figure 1. (a) Wind turbines in the U.S. portion of the Western Interconnection are located across a variety of ecoregions and show geographical variations of landforms (b) Annotation approach and the temporal variation of both turbine size and turbine spacing for two different projects: Directly-impacted land for older projects constructed before January 2003 (upper images) is segmented using a two-class scheme (i.e., background and actively-used), whereas for newer projects constructed after December 2002 (lower images), we used a three-class scheme (background, actively-used, and regenerating).

The main infrastructure elements of wind energy development include access roads, service roads, a circular surface land clearing for turbine installation, roadside clearing, and surface land clearing for buried cable. We simplify and categorize the land requirement by wind energy infrastructure into three classes, i.e., background, actively-used, and regenerating, based on their land occupation characteristics and visual appearance on imagery (Figure 1b). The background class is area not directly impacted by wind farm construction. The actively-used class includes access roads and service roads that shows a bright and smooth texture in an imagery. The regenerating class may include temporary roads, roadside clearings, temporary storage and laydown areas, land use by buried cable, and the circular clearing, which show a dim and rough texture in imagery. For older projects (typically before January 2003 in the WECC), we assume that the regenerating class has fully reclaimed and thus we use a two-class scheme (i.e., background and actively-used).

The workflow to determine land use via imagery segmentation includes three steps: deep learning model development, deep learning model application, and postprocessing.

Deep Learning Model Development. This step includes training set preparation, model training, and model validation. The images in the training set are discretely sampled according to the turbine locations across the study area to allow the deep learning model to recognize the various landscapes among wind projects. The training set was manually delineated in ArcGIS Pro supported by turbine location information from the USGS Wind Turbine Database. The manual recognition of NAIP pixel classes (e.g., whether a pixel should be categorized as background, actively-used, or regenerating) was aided by the reference world topographic map and world hill shade map in ArcGIS Pro.[47] In challenging landscapes, experts in the Expert Review Panel (see Acknowledgement) were consulted to ensure accuracy and quality. The training set preparation process and the delineation results were presented to the Expert Review Panel to guarantee the quality of the training set. >90% of the delineation was completed by the first author to ensure consistency using the quality assurance noted above. Detailed process of creating the training set can be found at Supplementary Note 1.

A dense version of U-Net network is used for training our model, which is an "encoder-decoder" type of architecture where the input image is translated to a low dimensional latent space using the encoder and then the decoder takes back the latent space to the image space to output the segmentation mask.[48] The encoder and decoder of the network consist of five blocks and each block consists of a dense convolutional block followed by batch normalization and ReLU non-linearity (Figure S1). U-Net is one of the most widely used deep-learning frameworks for image segmentation and has showed state-of-the art performance compared to its followers, as shown in recent studies in a variety of areas, including land-cover mapping.[49–52] There are max-pooling layers after each subsequent encoder block and upsampling layers after each subsequent decoder block. For upsampling, a simple bilinear interpolation operation is employed. The output segmentation mask is trained by supervising it with a cross-entropy loss over the ground truth. The network is trained for 400 epochs using Adam optimizer and a learning rate of 0.001. The network is developed and trained using the PyTorch framework on an NVIDIA RTX 8000 GPU. Notably, the following geographical processing is independent on the selection of deep learning method, so our framework is flexible to incorporate other image segmentation approaches.

We trained two separate dense U-Net models: one old project model and a new project model due to their differences in turbine size, turbine configuration, and vegetation reclaiming status. The old project model is trained on 301 images and their annotations (25 test images). The new project model is trained on 1687 images (75 test images). For validation, we separate the test data, which consists of manual annotations and are not part of the training dataset. The model performance is evaluated based on F1 score, which is defined as:

$$F1 = \frac{2TP}{2TP + FN + FP} \quad (1)$$

where TP, FN, and FP correspond to the number of true positives (i.e., correctly classified), false negatives (i.e., wrongly classified as another class), and false positives (i.e., wrongly classified from another class to the current class) in the output prediction, respectively. Detailed description of our model training can be found at Supplementary Note 2.

Model application and postprocessing are conducted on a cluster basis, with each cluster formed by a predefined minimum number of turbines, N_t, that are located within a search distance, d_s (Supplementary Note 3 provides further detail).

Energy Systems Analysis. We calculated the capacity-based LUE and land transformation of the selected projects based on the annual net generation from the U.S. Energy Information Administration and the USGS Wind Turbine Database (Version 3.0.1). As a variety of metrics have been used in energy systems analysis,[53,54] we selected capacity-based LUE and land transformation based on their frequency and acceptance of usage on comparative assessments of energy technologies and life cycle assessments.[55,56]

We use the EIA-860[57] and EIA-923[58] to identify the capacity factor of the wind turbines within the U.S. Wind Turbine Database. The capacity factor is the ratio of the actual amount of electricity generation to capacity-based generation. First year data has been neglected as turbines are usually not running steady in this period.[59] For turbines with missing turbine year or missing turbine capacity in the U.S. Wind Turbine Database, we assigned them with project averaged values. Projects with missing turbine information are listed in Supporting Data. Results from Hamilton et al. (2020) on the temporal trend of capacity factor were used when electricity generation data are not available from the EIA files.[59] A turbine lifetime of 30 years is assumed.

We compare capacity-based LUE among projects under three types of land-use circumstances: 1) the initial, which includes all the original construction land uses, 2) the reference-year (i.e., 2018), which represents the identified directly impacted area using the marchine-learning approach, and 3) the actively-used (or "permanent land use"), which includes only the land impacted by the actively used class and represents a scenario that the vegetation reclaiming process is completed. These three circumstances represent the reclamation process of the disturbance by project construction. We use results from the reference-year circumstance for agricultural projects and the initial circumstance results for other projects to compare the land transformation among projects for consistency considering the variation of project ages. The initial land use was obtained by adjusting the reference year land use to initial land use by applying the averaged measurements of the area of initial circular clearing, roadside clearing width, and width of clearing for buried cable.

Description of direct land use. Existing studies have focused on how the LUE of wind energy projects changes with variations in wind power project attributes, such as turbine capacity and year. However, we argue that to consistently identify patterns of LUE among wind farms, it is important to first limit the scope of the study to projects located at a comparable level of human modification due to the large variations in the composition of land-use elements. We limit our analysis to the core area of wind farms located in non-agricultural areas. The core area is defined as the area where turbines are connected by service roads but excluding the main access road.

We propose a site-residue model to describe the patterns of directly impacted land within the core area. This model decomposes the directly impacted land into two parts: the sites and the residues (Figure 2). The sites are assumed as linearly stacked and evenly distributed, forming into a single string. The area of such a string of sites can be estimated as a function of the turbine capacity. The difference between the real impacted area and the estimated impacted area between every two neighboring sites is defined as a residue. For example, for a wind project with parallel string configuration, the distance between strings of turbines is usually larger than twice the turbine spacing. In cluster configuration, multiple service roads are often observed. Further details on the model are documented in Supplementary Note 4.

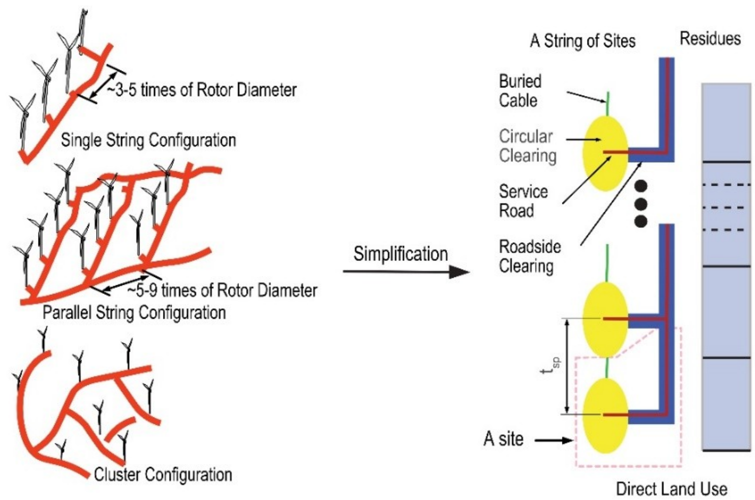

Figure 2. Directly impacted land by wind farms can be described as a combination of sites and residues.

The outreach impact of the turbines. We mapped and quantified the directly impacted land and the occupancy of surface land. However, the noise and visual impacts of turbines are not negligible, as the turbine diameter is greater than that of the circular clearing area. Researchers focused on energy systems planning have applied a buffer distance from 300 meters to 1,000 meters to quantify this effect, as summarized by Harrison-Atlas et al. (2022).[6] For large-scale studies, existing estimates also applied a universal buffer distance for all turbine sizes for convenience, regardless of the turbine diameter. Here, we examine the outreach impact of turbines by creating a buffer geometry extending from the directly impacted land that we determined using the deep learning approach. First, a circular buffer area is created around the turbine with a buffer distance from 1 to 10 times (step = 0.2) of the turbine diameter. Clusters of turbines without a valid rotor diameter in the USGS Wind Turbine Database were excluded from the analysis. The buffered geometry is then dissolved into the directly impacted land. This dissolving process merged the polygons from both the directly impacted land and the buffered geometry into a single polygon. We then calculated how the dissolve process impact the metrics by calculating the relative error of area $\left(RE_A\right)$ and relative error of LUE (RE_{LUE}¿, as follows:

$$\Re_A = \frac{A_{dissovled} - A_{buffer}}{A_{dissolved}}$$

$$\Re_{LUE} = \frac{LUE_{buffer} - LUE_{dissolved}}{LUE_{dissolved}}$$

where $A_{dissolved}$ and $LUE_{dissolved}$ are the area and LUE calculated from the dissolved polygon, respectively; and A_{buffer} and LUE_{buffer} are the area and LUE calculated from the buffered geometry around wind turbines, respectively.

Results and Discussions

Mapping of Directly Impacted Land by Wind Power Development. Our framework combines imagery analysis with machine learning to support efficient and accurate large-scale land-use mapping of wind energy infrastructure. We mapped the directly impacted land of more than 300 wind farms (>15,000 Turbines) in the U.S. part of the Western Interconnection by processing >90,000 images with an average processing speed of ~1.85 seconds/image, and where each image represents an area from ~1.05 km^2 to ~0.26 km^2 (imagery resolution 1- 0.5 m, respectively) (Table S1).

Our workflow achieved at least 99% accuracy in quantifying the area of directly impacted land without manual delineation. By segmenting the imagery into background and directly impacted land, the deep learning models identify the directly impacted land from background land cover with a median background F1 score of 99.6% for old projects and 99.8% for new projects (i.e., demonstrating high performance). The median F1 score for the three-class classification scheme (i.e., background, actively-used, and regenerating) is 96.4% for the clearing class and 96.2% for the actively-used class. The classification error mainly came from the actively-used class being classified as background class (Figure S6).

The machine learning model substantially reduces the time and effort required for obtaining the directly impacted land for wind farms. By employing machine learning, >99% workload has been reduced compared to manual delineation since our model correctly identified the majority of areas of interest, especially for the entire road network, and the remaining <1% workload is related to identifying false negatives and false positives (e.g., making up the circular clearing and removing noise in background). Due to the common existence of colocation in wind farms, manual delineation is and will be a general required step to obtain the directly impacted land for solving tasks of differentiating the purposes of land with the same land use class. For example, a machine learning model can extract all the road pixels for a wind power project located in agricultural area but determining which roads are used by a wind farm needs human determination. The accuracy of automatic classification is critical for obtaining final results efficiently since processing inaccurate automated extraction results costs more time compared to pure manual processing. Compared to processing imagery with a similar resolution with an area over 64 km^2, our approach uses only 0.2% to 1.6% of the time required for the existing commercial automated extraction tools.[26]

Characteristics of Land Use in Wind Farms. Based on the human modification level in the project area, we categorized the wind farms into four types: Access Road, No Access Road, Agricultural Area, and Mixed, to show how a different configuration of land-use elements impacts the performance of LUE (Figure 3a and Figure S2-S5). An Access Road project, located in an area with minor human disturbances, requries the construction of an access road to connect the wind farm region with existing road network. An access road is not required for the No Access Road projects since they utilize existing road. Agricultural Area projects are entirely or partially situated within agricultural production areas, where most of the land has been modified by human activities. Mixed projects are a mix of old and new wind farms in the same area. Since the turbine size in old projects is much smaller (~1/3 in terms of rotor diameter), only part of the existing infrastructures can be utilized for the construction of new wind farms. Service roads and circular clearings are usually still required to construct the new projects.

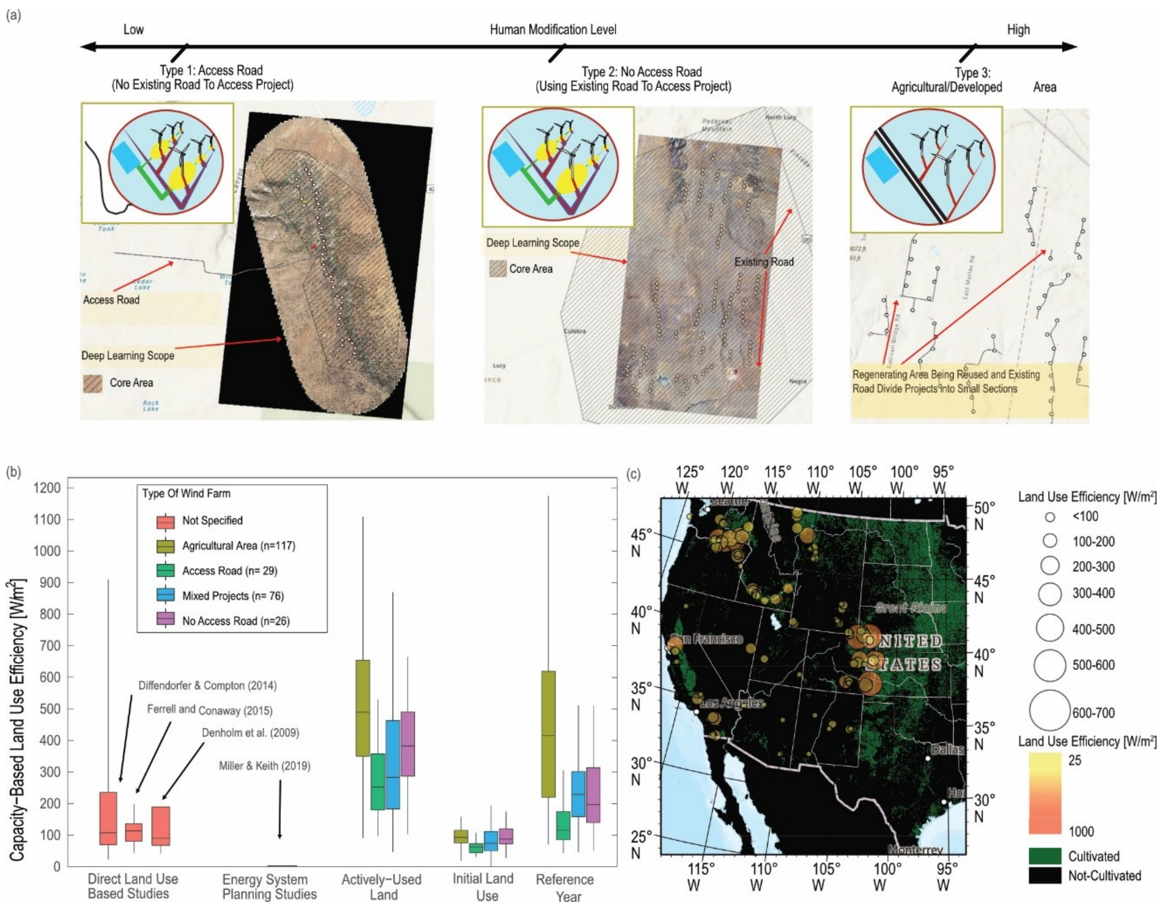

Figure 3. (a) Three types of wind farms based on the level of human modification in the project area. (b) The distribution of capacity based LUE. "Mixed Projects" are a mixed of new projects and old projects in the same area. "Actively-Used Land" represents a scenario with only actively-used class being occupied and all regenerating class are reclaimed. "Initial Land Use" is a scenario where all the initial disturbances are considered. "Reference Year" considers land use in the reference year of this study (2018) (c) The spatial distribution of LUE in the Western Interconnection.

Our results reveal that the key to improve the capacity-based LUE is to utilize existing roads (Figure 4b). In all three circumstances, Access Road projects have the lowest capacity-based LUE (a mean of 63.8 with 95% confidence interval of ±8.9 W/m^2 in initial circumstance and 275±43.6 W/m^2 in actively-used circumstance). Access roads can account for up to ~70% and a mean of ~25% of the total road length for the Access Road projects. Being able to share access/service roads with agricultural production activities, the Agricultural Area projects have a capacity-based LUE of 95.5± 6.0 W/m^2 under the initial circumstance, which is comparable to the No Access Road type and the Mixed type (98.7±17.9 W/m^2 and 80.4±9.8 W/m^2, respectively). Benefited from the capability of reusing a majority of the disturbed land (e.g., the circular clearing and land above buried cables), the capacity-based LUE of the Agricultural Area type in the reference-year circumstance achieves 447±49.4 W/m^2, close to their actively-used circumstance (517±44.5 W/m^2). Another reason for the high LUE of the Agricultural Area type is that the service road can be very short and connects only 1-2 turbines. The capacity-based LUE of Mixed type is 80.4±9.8 W/m^2 in the initial circumstance and rises to 256±34.7W/m^2 in the reference-year circumstance. The increase can be attributed to the fully reclaimation of land for projects built before 2003.

Similarly, our results show that the projects of the Mixed type and the Access Road type have higher land transformation (0.27±0.06 m^2/MWh and 0.24±0.07 m^2/MWh, respectively). While the higher land transformation of Access Road type is from its higher initial land use, compared to No Access Road which has a land transformation of 0.16±0.05 m^2/MWh), the land transformation of Mixed type (0.28±0.04 m^2/MWh) is driven by their low lifetime generation. This may be because of the Mixed projects' low capacity factor due to the existence of the older models of turbines. The Mixed type also has a higher variation in land transformation, with the medium land transformation lower than the Access Road type. Wind farms in agricultural area, as expected, have the lowest land transformation at 0.05±0.01 m^2/MWh.

The range of our results for capacity-based LUE are consistent with the results of the previous manual delineation studies (e.g., Diffendorfer and Compton (2014)[20] and Ferrel and Conaway (2015)[11]) and the Mixed type with a majority of projects built before 2003 shows consistency with the estimation of Denholm et al. (2009)[15]. Estimates using a geoprocessing-based approach, however, could be significantly lower, to ~2.8 W/m^2, which is due to the directly impacted land in our study is only portion of the zones (e.g., the Theissen polygons or circular buffered areas). .

It should be noted that, although we mapped the directly impacted land for 132 Agricultural Area projects, 84 Mixed projects, 50 Access Road projects, and 39 No Access Road projects, metrics can only be calculated for a portion of the projects when the required data (e.g., turbine capacity) are available.

Understanding the Variability in the Directly Impacted Land. Our results suggest that the LUE of wind farms is positively coupled with turbine capacity and is related to the number of turbines in a farm. Area of a site, as defined in Figure 2, is mainly related to two factors: turbine spacing and the radius of circular clearing. Estimation of minimum turbine spacing (Eq. S9 and Eq. S10) suggests that existing turbines are not necessarily spaced at the optimum suggested distance (Figure S12a). Circular clearing is less dependent on turbine rotor diameter and has a smaller variation compared to turbine spacing. The relationships with other land-use elements can be regarded as minor. As a result, under current wind project configurations, the increase of turbine capacity is higher than the increase of the site area, which leads to the increase of LUE as turbine rotor diameter increases.

When accounting for the residues, we found that as turbine capacity increases, both the area of residues and the proportion of site area out of total area increases. Therefore, for projects with a fixed number of turbines, the LUE increases as turbine capacity increases (Eq. S8). For projects with turbines of a capacity less than 0.5 MW, the residue area is ~200% the site area. For wind farms built before 2003, the turbine spacing can be barely larger than the rotor diameters and there are circumstances where the service roads do not connect two turbines directly but instead form a "claw" shape, which increases the total residue area. When turbines are larger than 1.5 MW, the residue area remains steady, and the site area increases as to the turbine spacing increases (Figure S12b). This could be due to the service road length per turbine nearing the distance between turbines, resulting in a reduced fraction of additional service road needed (Figure S7). The area of several sites exhibits a decline for projects using turbines with a capacity >3 MW as these turbines are located closer than those with smaller capacities (Figure S12a).

We observed that projects with a small number of wind turbines (<6 typically) have a much higher LUE as turbines in such projects can form a single line of sites. As the number of turbines increases, an increasing residue area is often required to form multiple lines of turbines (e.g., a parallel configuration). So, for projects with a fixed turbine capacity, it is reasonable to assume that, as the number of turbines increases, the ratio of the site area to the residue area is constant or decreases, which can thus lead to a decrease in LUE. However, we did not see this trend. Projects with similar turbine capacity appear to have a similar LUE as the project capacity increase (Figure S12c). One potential reason is that as the number of turbines increases, the ratio of turbine spacing to turbine rotor diameter decreases (Figure S8).

Parametric buffer analysis and rotor diameter. By parametrically increasing the buffer distance surrounding the turbine, the margin of error of LUE based on buffering geometry diminishes exponentially (Figure 4a). When the buffer factor exceeds four, the discrepancy between both RE_A and RE_{LUE}falls below 5% for all projects. When employing methods that rely on buffering geometry to quantify LUE, large errors arise for wind farms located in areas with little human modification due to the larger amount directly impacted land (e.g., the additional land use by the access roads).

With increasing buffer distance, the directly impacted area becomes inconsequential due to two factors. First, the buffered geometry completely covers the directly impacted land (i.e., the circular clearing and service roads are dissolved into the geometry). Second, the magnitude of land-use components is minuscule in comparison to the buffer diameter. Manual measurements indicate that the width of service roads, roadside clearings, and cable remains relatively diminutive and consistent among projects, with maximum magnitudes not exceeding 15 meters, 18 meters, and 17 meters, respectively. Conversely, the magnitude of turbine diameter can be an order of magnitude greater for larger turbines. Regardless, specific land uses, such as agriculture, occur right up to the base of the turbine, rendering the buffer a meaningless proxy for specific impacts.

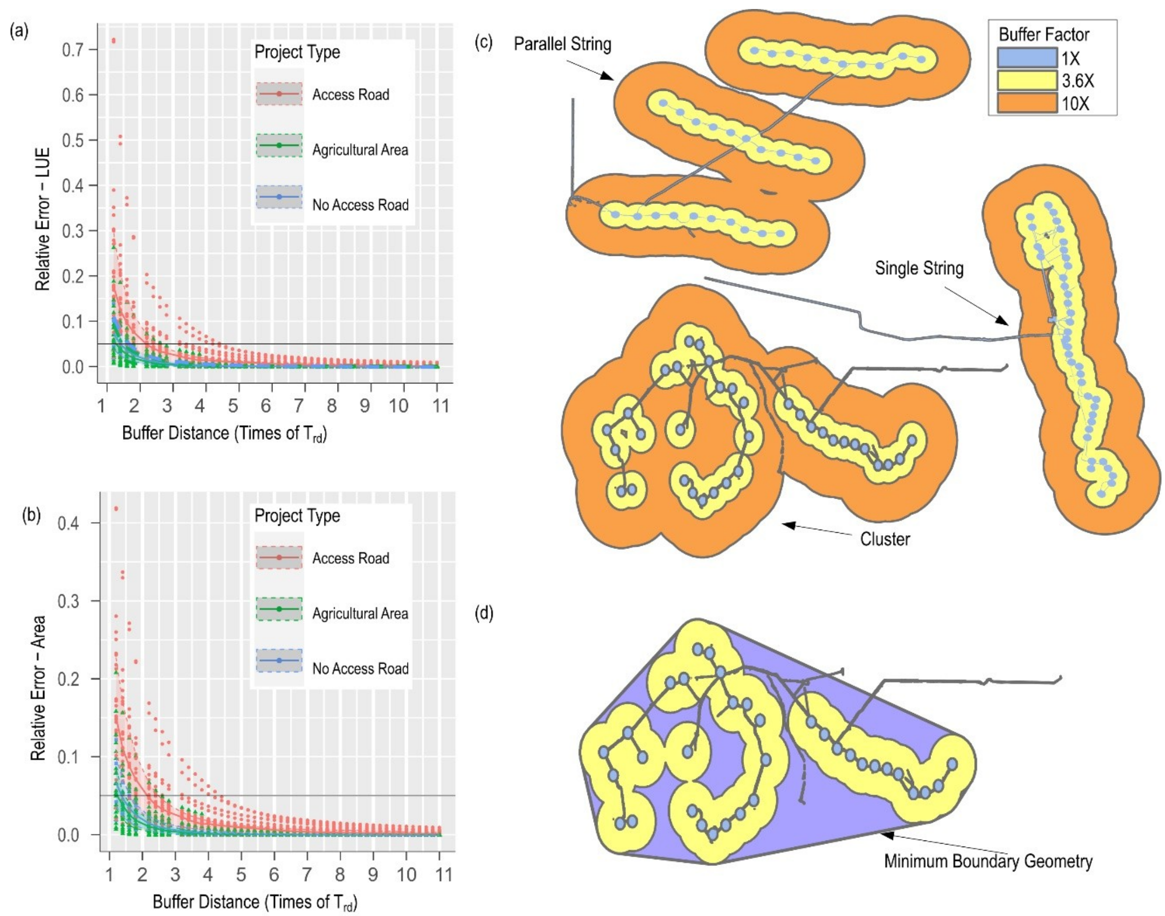

Figure 4. (a) The changes of the relative error of land use efficiency (LUE) with buffer distance (b) The changes of the relative error of area with buffer distance (c) Impact of buffer distance on the impacted area for different wind turbine configurations (d) Minimum bounding geometry could be applied for estimating land use when the turbine impact is considered as small to fill the holes in the impacted area.

Furthermore, the accuracy of buffer-based methodologies is contingent upon the configuration of the turbines (Figure 4). For a smaller buffering factor (e.g., 1X), there is an absence of overlap among the buffered geometry, rendering the geometry unsuitable for evaluating the land-use impact, except in instances where the gaps between turbines are occupied by pre-existing infrastructure, such as in developed or agricultural areas. For single string and parallel string configurations, as buffering factor increases, the buffered geometry overlaps and dissolves (Figure 4c). Service roads are dissolved into the buffer-based geometry and only a minuscule fraction of the area is excluded from these areas. In such cases, the land-use area serves as an adequate proxy for directly impacted land.

For projects with a cluster configuration, when the buffering factor is not large enough, additional analysis may be necessary, as additional gaps or holes can be generated within the impacted areas (Figure 4c). Another option for obtaining the amount of land-use is to create a minimum bounding convex polygon (Figure 4d), as have been applied in previous studies in energy system planning oriented studies.[43] The minimum bounding geometry is dependent on the configuration of projects and includes all of the area between turbines. However, a large fraction of undisturbed land (e.g., the purple pixels in Figure 4d) is likely to be included with a convex polygon approach. The magnitude of error could increase when the buffering distance increases.

The buffering distance and the configuration of turbines are thus critical factors to accurately assess the land-use impact of an existing wind farm. If the regionalized impact from a turbine is considered as small (e.g., <4 times of rotor diameter), it is important to obtain the directly impacted land to avoid overestimating the land-use impact in areas with high levels of human modification and to avoid underestimating it in areas with low levels of human modification. Further analysis on the uncertainty of our method is documented in Supplementary Note 5.

Future Research and Contribution

The workflow we developed can serve as a prototype for mapping the land use of wind farms in other regions and other types of energy projects. The current workflow involves manual delineation work in both training set preparation and post processing (Table S2). We chose manual processing to solve the challenges associated with co-location of wind power and other human activities. In addition, we opted for manual processing because our primary goal is achieving accurate land-use mapping. The current model helped mitigate the majority of workload. Although the deep learning model can be potentially improved by adding new annotated images, there is a tradeoff between model performance and overall time consumption. Limited by resource and time, the performance of the existing model could be inadequate for land-cover types that are beyond the geographical scope (i.e., the WECC). In such a case, our post-processed results can be used as an additional training set. Region-specified training set can also be obtained based on the documented steps in Supplementary Note 1. Similar to wind turbines, oil/natural gas production wells/pads are also dispersedly distributed across landscape, and due to the longer history and >2 orders larger number of facilities, automated approaches are in demand for quantifying land use by oil/natural gas production to understand the landscape consequences as manual delineation is still a main approach for land use quantification.[27,60,61] Due to the dearth of data, natural gas infrastructure is generally compared to the entire wind farm in planning studies, rather than solely the infrastructure for wind.[62] The utilization of these values yields incommensurable results, potentially misleading decision-makers. This research fills a much-needed gap in LCA and planning inventories that will enable more robust examination of new and developing impact assessment methods.

The significance of this study lies in its introduction of an approach that enables spatially explicit, empirical measurement of the direct land impacted by wind power at a large scale. The analysis utilizes a machine learning approach to enable the development of data inventories critical to the analysis of large-scale and regional impacts of wind development; for example, such inventories have not ever before been developed for use in life cycle assessment and planning studies. Importantly, we have also defined the key concepts and impact factors involved in identifying patterns of land-use by wind energy. Combined with recent studies,[27] results set the stage for the first consistent comparisons on environmental sustainability across different energy technologies, whether in the context of LCA, environmental impact analysis or energy systems planning for net zero emissions.

Supporting Information

Additional results, methodology description, and supplementary notes are documented in Supporting Information.docx.

Wind farms with missing turbine information, classification of wind farms, image sources, land transformation, and land use efficiency are documented in Supporting Data.xlsx. Postprocessed results at a cluster level are stored at supporting_map.gdb.

Author Information

Corresponding author

Sarah M Jordaan, Ph.D. – McGill University, Montreal QC, H3A 1E3, Canada

Email: sarah.jordaan@mcgill.ca

Authors

Tao Dai - School of Advanced International Studies, Johns Hopkins University, Washington, DC, 20036, USA; Joint BioEnergy Institute, Lawrence Berkeley National Laboratory, Emeryville, CA 94608, USA

Jeya M Jose - Department of Electrical and Computer Engineering, Johns Hopkins University, Baltimore, Maryland, 21218, USA

Yifan Zhao - Department of Environmental Health and Engineering, Johns Hopkins University, Baltimore, Maryland, 21218, USA

Shuwen Zheng- Department of Electrical and Computer Engineering, Johns Hopkins University, Baltimore, Maryland, 21218, USA

Yinong Sun - Department of Environmental Health and Engineering, Johns Hopkins University, Baltimore, Maryland, 21218, USA

Vishal M Patel - Department of Electrical and Computer Engineering, Johns Hopkins University, Baltimore, Maryland, 21218, USA

Author Contributions: TD, JMJ, VMP, and SMJ designed the research, TD and JMJ performed research, TD and JMJ contributed new reagents/analytic tools, TD analyzed data, TD, JMJ and SMJ wrote the paper.

Acknowledgments. This research was supported by the Alfred P. Sloan Foundation. We acknowledge the feedback on our research and generosity of time provided by an external expert review panel, comprised of government, non-profit, industry, and academics. Experts included Timothy Skone, Jim Kuiper, Garvin Heath, Matthew Bailey, Barry Woertz, Benjamin Riggan, Rama Chappella, James O'Sullivan, Christopher Newman, Tim Hayes, Rebecca Hernandez, Jane Long, Armond Cohen, and Anders Johnson. We also acknowledge Johns Hopkins support from IDIES (Gerard Lemson and Alexander Szalay), in GIS training (Bonni Wittstadt), and from colleagues (Ben Hobbs). Tao Dai thanks the support of the U.S. Department of Energy (DOE) Office of Science and Office of Fossil Energy and Carbon Management under Contract No. DE-AC02-05CH11231. The United States Government retains and the publisher, by accepting the article for publication, acknowledges that the United States Government retains a nonexclusive, paid-up, irrevocable, world-wide license to publish or reproduce the published form of this manuscript, or allow others to do so, for United States Government purposes.

Data Availability. Manually annotated images will be shared upon request.

References

(1) Jenkins, J. D.; Mayfield, E. N.; Larson, E. D.; Pacala, S. W.; Greig, C. Mission Net-Zero America: The Nation-Building Path to a Prosperous, Net-Zero Emissions Economy. *Joule* **2021**, *5* (11), 2755–2761.

(2) Wang, F.; Harindintwali, J. D.; Yuan, Z.; Wang, M.; Wang, F.; Li, S.; Yin, Z.; Huang, L.; Fu, Y.; Li, L. Technologies and Perspectives for Achieving Carbon Neutrality. *Innov.* **2021**, *2* (4), 100180.

(3) U.S. Energy Information Administration. Annual Energy Outlook 2022 https://www.eia.gov/outlooks/aeo/ (accessed Dec 31, 2021).

(4) Baker, S. E.; Stolaroff, J. K.; Peridas, G.; Pang, S. H.; Goldstein, H. M.; Lucci, F. R.; Colin, M. *Getting to Neutral. Options for Negative Carbon Emissions in California*; 2020.

(5) Madhu, K.; Pauliuk, S.; Dhathri, S.; Creutzig, F. Understanding Environmental Trade-Offs and Resource Demand of Direct Air Capture Technologies through Comparative Life-Cycle Assessment. *Nat. Energy* **2021**, *6* (11), 1035–1044. https://doi.org/10.1038/s41560-021-00922-6.

(6) Harrison-Atlas, D.; Lopez, A.; Lantz, E. Dynamic Land Use Implications of Rapidly Expanding and Evolving Wind Power Deployment. *Environ. Res. Lett.* **2022**, *17* (4), 044064. https://doi.org/10.1088/1748-9326/ac5f2c.

(7) Miller, L. M.; Keith, D. W. Addendum: Observation-Based Solar and Wind Power Capacity Factors and Power Densities (Environ. Res. Lett. (2018) 13 (104008) DOI: 10.1088/1748-9326/Aae102). *Environ. Res. Lett.* **2019**, *14* (7). https://doi.org/10.1088/1748-9326/ab12a2.

(8) Bolinger, M.; Bolinger, G. Land Requirements for Utility-Scale PV: An Empirical Update on Power and Energy Density. *IEEE J. Photovoltaics* **2022**, *12* (2), 589–594. https://doi.org/10.1109/JPHOTOV.2021.3136805.

(9) Mai, T.; Wiser, R.; Sandor, D.; Brinkman, G.; Heath, G.; Denholm, P.; Hostick, D. J.; Darghouth, N.; Schlosser, A. Strzepek, K. *Renewable Electricity Futures Study: Exploration of High-Penetration Renewable Electricity Futures*; Golden, CO, 2012; Vol. 1.

(10) Lovering, J.; Swain, M.; Blomqvist, L.; Hernandez, R. R. Land-Use Intensity of Electricity Production and Tomorrow's Energy Landscape. *PLoS One* **2022**, *17* (7 July), 1–17. https://doi.org/10.1371/journal.pone.0270155.

(11) Ferrell, S. L.; Conaway, J. *Wind Energy Industry Impacts in Oklahoma*; 2015.

(12) Strickland, D.; Johnson, D. Overview of What We Know About Avian/Wind Interaction. In *National Wind Coordinating Collaborative Wildlife Workgroup Research Meeting VI*; 2006.

(13) Bureau of Land Management. *Final Programmatic Environmental Impact Statement on Wind Energy Development on BLM Administered Land in the Western United States*; 2005.

(14) Rand, J. T.; Kramer, L. A.; Garrity, C. P.; Hoen, B. D.; Diffendorfer, J. E.; Hunt, H. E.; Spears, M. A Continuously Updated, Geospatially Rectified Database of Utility-Scale Wind Turbines in the United States. *Sci. Data* **2020**, *7* (1), 1–12. https://doi.org/10.1038/s41597-020-0353-6.

(15) Denholm, P.; Hand, M.; Jackson, M.; Ong, S. *Land Use Requirements of Modern Wind Power Plants in the United States*; 2009; Vol. Technical. https://doi.org/10.2172/964608.

(16) Walker, B. L.; Neubaum, M. A.; Goforth, S. R.; Flenner, M. M. Quantifying Habitat Loss and Modification from Recent Expansion of Energy Infrastructure in an Isolated, Peripheral Greater Sage-Grouse Population. *J. Environ. Manage.* **2020**, *255*. https://doi.org/10.1016/j.jenvman.2019.109819.

(17) Johnson, N. *Pennsylvania Energy Impacts Assessment. Report 1: Marcellus Shale Natural Gas and Wind*; 2010.

(18) Milheim, L. E.; Slonecker, E. T.; Roig-Silva, C. M.; Malizia, A. R. *Landscape Consequences of Natural Gas Extraction in Lackawanna and Wayne Counties, Pennsylvania, 2004-2010: U.S. Geological Survey Open-File Report 2013-1227, 32 P.*; Reston, Virginia, 2013.

(19) Milheim, L. E.; Slonecker, E. T.; Roig-Silva, C. M.; Malizia, A. R. *Landscape Consequences of Natural Gas Extraction in Lackawanna and Wayne Counties Open-File Report 2013-1227*; 2004.

(20) Diffendorfer, J. E.; Compton, R. W. Land Cover and Topography Affect the Land Transformation Caused by Wind Facilities. *PLoS One* **2014**, *9* (2). https://doi.org/10.1371/journal.pone.0088914.

(21) Murray, A. G.; Mills, B. F. Read the Label! Energy Star Appliance Label Awareness and Uptake among U.S. Consumers. *Energy Econ.* **2011**, *33* (6), 1103–1110. https://doi.org/10.1016/j.eneco.2011.04.013.

(22) Lopez, A.; Roberts, B.; Heimiller, D.; Blair, N.; Porro, G. U.S. Renewable Energy Technical Potentials: A GIS-Based Analysis. *Natl. Renew. Energy Lab. Doc.* **2012**, *1* (7), 1–40.

(23) Lopez, A.; Mai, T.; Lantz, E.; Harrison-Atlas, D.; Williams, T.; Maclaurin, G. Land Use and Turbine Technology Influences on Wind Potential in the United States. *Energy* **2021**, *223*, 120044. https://doi.org/10.1016/j.energy.2021.120044.

(24) Lopez, A.; Cole, W.; Sergi, B.; Levine, A.; Carey, J.; Mangan, C.; Mai, T.; Williams, T.; Pinchuk, P.; Gu, J. Impact of Siting Ordinances on Land Availability for Wind and Solar Development. *Nat. Energy* **2023**. https://doi.org/10.1038/s41560-023-01319-3.

(25) Diffendorfer, J. E.; Dorning, M. A.; Keen, J. R.; Kramer, L. A.; Taylor, R. V. Geographic Context Affects the Landscape Change and Fragmentation Caused by Wind Energy Facilities. *PeerJ* **2019**, *2019* (7). https://doi.org/10.7717/peerj.7129.

(26) Germaine, S. S.; O'donnell, M.; Aldridge, C. L.; Baer, L.; Fancher, T.; Mcbeth, J.; Mcdougal, R. R.; Waltermire, R.; Bowen, Z. H.; Diffendorfer, J.; Garman, S.; Hanson, L. *Mapping Surface Disturbance of Energy-Related Infrastructure in Southwest Wyoming-An Assessment of Methods*; Reston, Virginia, 2012.

(27) Dai, T.; Valanarasu, J. M. J.; Patel, V. M.; Jordaan, S. M. The Life Cycle Land Use of Natural Gas-Fired Electricity in the US Western Interconnection. *Environ. Sci. Adv.* **2023**, 815–826. https://doi.org/10.1039/d3va00038a.

(28) Campos-Taberner, M.; García-Haro, F. J.; Martínez, B.; Izquierdo-Verdiguier, E.; Atzberger, C.; Camps-Valls, G.; María, &; Gilabert, A. Understanding Deep Learning in Land Use Classification Based on Sentinel-2 Time Series. **2020**. https://doi.org/10.1038/s41598-020-74215-5.

(29) Wu, A. N.; Biljecki, F. Roofpedia: Automatic Mapping of Green and Solar Roofs for an Open Roofscape Registry and Evaluation of Urban Sustainability. *Landsc. Urban Plan.* **2021**, *214*. https://doi.org/10.1016/J.LANDURBPLAN.2021.104167.

(30) Yu, J.; Wang, Z.; Majumdar, A.; Rajagopal, R. DeepSolar: A Machine Learning Framework to Efficiently Construct a Solar Deployment Database in the United States. **2018**. https://doi.org/10.1016/j.joule.2018.11.021.

(31) Parhar, P.; Sawasaki, R.; Nusaputra, N.; Vergara, F.; Todeschini, A.; Vahabi, H. HyperionSolarNet Solar Panel Detection from Aerial Images.

(32) Kruitwagen, L.; Story, K. T.; Friedrich, J.; Byers, L.; Skillman, S.; Hepburn, C. A Global Inventory of Photovoltaic Solar Energy Generating Units. *Nature* **2021**, *598* (7882), 604–610. https://doi.org/10.1038/S41586-021-03957-7.

(33) Jordaan, S. M.; Heath, G. A.; Macknick, J.; Bush, B. W.; Mohammadi, E.; Ben-Horin, D.; Urrea, V.; Marceau, D. Understanding the Life Cycle Surface Land Requirements of Natural Gas-Fired Electricity. *Nat. Energy* **2017**, *2* (10), 804–812. https://doi.org/10.1038/s41560-017-0004-0.

(34) Dai, T.; Jordaan, S. M.; Wemhoff, A. P. Gaussian Process Regression as a Replicable, Streamlined Approach to Inventory and Uncertainty Analysis in Life Cycle Assessment. *Environ. Sci. Technol.* **2022**, *56* (6), 3821–3829. https://doi.org/10.1021/acs.est.1c04252.

(35) De Baan, L.; Mutel, C. L.; Curran, M.; Hellweg, S.; Koellner, T. Land Use in Life Cycle Assessment: Global Characterization Factors Based on Regional and Global Potential Species Extinction. *Environ. Sci. Technol.* **2013**, *47* (16), 9281–9290. https://doi.org/10.1021/es400592q.

(36) Koellner, T.; Baan, L.; Beck, T.; Brandão, M.; Civit, B.; Margni, M.; Canals, L. M.; Saad, R.; Souza, D. M.; Müller-Wenk, R. UNEP-SETAC Guideline on Global Land Use Impact Assessment on Biodiversity and Ecosystem Services in LCA. *Int. J. Life Cycle Assess.* **2013**, *18* (6), 1188–1202. https://doi.org/10.1007/s11367-013-0579-z.

(37) Hellweg, S.; Canals, L. M. I. Emerging Approaches, Challenges and Opportunities in Life Cycle Assessment. *Science (80-.).* **2014**, *344* (6188), 1109–1113. https://doi.org/10.1126/science.1248361.

(38) Jordaan, S. M.; Combs, C.; Guenther, E. Life Cycle Assessment of Electricity Generation: A Systematic Review of Spatiotemporal Methods. *Adv. Appl. Energy* **2021**, *3* (July), 100058. https://doi.org/10.1016/j.adapen.2021.100058.

(39) Cooney, G.; Jamieson, M.; Zaimes, G. G. *Development of an Open-Source Life Cycle Baseline for Electricity Consumption in the United States-LCAXIX*; National Energy Technology Laboratory (NETL), Pittsburgh, PA, Morgantown, WV …, 2019.

(40) Cooney, G.; Skone, T. J.; Jamieson, M.; Zaimes, G. G. Open-Source Life Cycle Baseline for Electricity Consumption in the United States-LCI Public Release. In *AGU Fall Meeting Abstracts*; 2019; Vol. 2019, pp A41D-04.

(41) Nelson, E.; Mendoza, G.; Regetz, J.; Polasky, S.; Tallis, H.; Cameron, D. R.; Chan, K. M. A.; Daily, G. C.; Goldstein, J.; Kareiva, P. M.; Lonsdorf, E.; Naidoo, R.; Ricketts, T. H.; Shaw, M. R. Modeling Multiple Ecosystem Services, Biodiversity Conservation, Commodity Production, and Tradeoffs at Landscape Scales. *Front. Ecol. Environ.* **2009**, *7* (1), 4–11. https://doi.org/10.1890/080023.

(42) Jones, N. F.; Pejchar, L.; Kiesecker, J. M. The Energy Footprint: How Oil, Natural Gas, and Wind Energy Affect Land for Biodiversity and the Flow of Ecosystem Services. *Bioscience* **2015**, *65* (3), 290–301. https://doi.org/10.1093/biosci/biu224.

(43) Jones, N. F.; Pejchar, L. Comparing the Ecological Impacts of Wind and Oil & Gas Development: A Landscape Scale Assessment. *PLoS One* **2013**, *8* (11). https://doi.org/10.1371/journal.pone.0081391.

(44) Crooks, K. R.; Burdett, C. L.; Theobald, D. M.; King, S. R. B.; Di Marco, M.; Rondinini, C.; Boitani, L. Quantification of Habitat Fragmentation Reveals Extinction Risk in Terrestrial Mammals. *Proc. Natl. Acad. Sci. U. S. A.* **2017**, *114* (29), 7635–7640. https://doi.org/10.1073/pnas.1705769114.

(45) The Western Electricity Coordinating Council (WECC). *2016 State of the Interconnection*; 2016.

(46) U.S. Fish and Wildlife Service. ECOS: Environmental Conservation Online System https://ecos.fws.gov/ecp/ (accessed Jun 22, 2021).

(47) Esri. World Topographic Map https://www.arcgis.com/home/item.html?id=7dc6cea0b1764a1f9af2e679f642f0f5.

(48) Ronneberger, O.; Fischer, P.; Brox, T. U-Net: Convolutional Networks for Biomedical Image Segmentation. In *International Conference on Medical image computing and computer-assisted intervention*; Springer, 2015; pp 234–241.

(49) Solórzano, J. V.; Mas, J. F.; Gao, Y.; Gallardo-Cruz, J. A. Land Use Land Cover Classification with U-Net: Advantages of Combining Sentinel-1 and Sentinel-2 Imagery. *Remote Sens.* **2021**, *13* (18), 3600. https://doi.org/10.3390/RS13183600/S1.

(50) Zhang, W.; Tang, P.; Zhao, L. Fast and Accurate Land-Cover Classification on Medium-Resolution Remote-Sensing Images Using Segmentation Models. *Int. J. Remote Sens.* **2021**, *42* (9), 3277–3301. https://doi.org/10.1080/01431161.2020.1871094.

(51) Sun, P.; Lu, Y.; Zhai, J. Mapping Land Cover Using a Developed U-Net Model with Weighted Cross Entropy. https://doi.org/10.1080/10106049.2021.2017017.

(52) Li, Y.; Zhou, Y.; Zhang, Y.; Zhong, L.; Wang, J.; Chen, J. DKDFN: Domain Knowledge-Guided Deep Collaborative Fusion Network for Multimodal Unitemporal Remote Sensing Land Cover Classification. *ISPRS J. Photogramm. Remote Sens.* **2022**, *186*, 170–189. https://doi.org/10.1016/J.ISPRSJPRS.2022.02.013.

(53) Wachs, E.; Engel, B. Land Use for United States Power Generation: A Critical Review of Existing Metrics with Suggestions for Going Forward. *Renew. Sustain. Energy Rev.* **2021**, *143* (February). https://doi.org/10.1016/j.rser.2021.110911.

(54) Cagle, A. E.; Shepherd, M.; Grodsky, S. M.; Armstrong, A.; Jordaan, S. M.; Hernandez, R. R. Standardized Metrics to Quantify Solar Energy-Land Relationships: A Global Systematic Review . *Frontiers in Sustainability* . 2023.

(55) Smil, V. Power Density Primer: Understanding the Spatial Dimension of the Unfolding Transition to Renewable Electricity Generation (Part I-Definitions). **2010**.

(56) Hernandez, R. R.; Hoffacker, M. K.; Field, C. B. Land-Use Efficiency of Big Solar. *Environ. Sci. Technol.* **2014**, *48* (2), 1315–1323. https://doi.org/10.1021/es4043726.

(57) U.S. Energy Information Administration. Form EIA-860 detailed data with previous form data (EIA-860A/860B) https://www.eia.gov/electricity/data/eia860/ (accessed Nov 26, 2021).

(58) Form EIA-923 detailed data with previous form data (EIA-906/920) https://www.eia.gov/electricity/data/eia923/ (accessed Nov 26, 2021).

(59) Hamilton, S. D.; Millstein, D.; Bolinger, M.; Wiser, R.; Jeong, S. How Does Wind Project Performance Change with Age in the United States? *Joule* **2020**, *4* (5), 1004–1020. https://doi.org/10.1016/j.joule.2020.04.005.

(60) Chomphosy, W. H.; Varriano, S.; Lefler, L. H.; Nallur, V.; McClung, M. R.; Moran, M. D. Ecosystem Services Benefits from the Restoration of Non-Producing US Oil and Gas Lands. *Nat. Sustain.* **2021**, *4* (6), 547–554. https://doi.org/10.1038/s41893-021-00689-4.

(61) Johnson, N.; Gagnolet, T.; Ralls, R.; Stevens, J. *Natural Gas Pipelines. Excerpt from Report 2 of the Pennsylvania Energy Impacts Assessment*; 2011.

(62) Palmer-Wilson, K.; Donald, J.; Robertson, B.; Lyseng, B.; Keller, V.; Fowler, M.; Wade, C.; Scholtysik, S.; Wild, P.; Rowe, A. Impact of Land Requirements on Electricity System Decarbonisation Pathways. *Energy Policy* **2019**, *129* (January), 193–205. https://doi.org/10.1016/j.enpol.2019.01.071.